

Article

Luminescent Diimine-Pt(IV) Complexes with Axial Phenyl Selenide Ligands

Marzieh Dadkhah Aseman^{1,*}, Reza Babadi Aghakhanpour¹, Zohreh Sharifioliaei², Axel Klein^{3,*}
and S. Masoud Nabavizadeh^{3,4}

¹ Faculty of Sciences, Department of Chemistry, Tarbiat Modares University, Tehran 15719-14911, Iran; r.babadi.a@gmail.com

² Faculty of Chemistry, Kharazmi University, Tehran 15719-14911, Iran; sharifi.zohreh1996@gmail.com

³ Faculty of Mathematics and Natural Sciences, Department of Chemistry and Biochemistry, Institute for Inorganic Chemistry, University of Cologne, Greinstrasse 6, D-50939 Köln, Germany; nabavizadeh@shirazu.ac.ir

⁴ Professor Rashidi Laboratory of Organometallic Chemistry, Department of Chemistry, College of Sciences, Shiraz University, Shiraz 71467-13565, Iran

* Correspondence: m.dadkhah@modares.ac.ir (M.D.A.); axel.klein@uni-koeln.de (A.K.)

Abstract: Luminescent diimine-Pt(IV) complexes [Pt(N[∞]N)(Me)₂(PhSe)₂], (N[∞]N = 2,2'-bipyridine (**1b**), 1,10-phenanthroline (**phen**, **2b**), and 4,4'-dimethyl-2,2'-bipyridine (Me₂bpy, **3b**), PhSe[−] = phenyl selenide were prepared and identified using multinuclear (¹H, ¹³C{¹H} and ⁷⁷Se{¹H}) NMR spectroscopy. The PhSe[−] ligands were introduced through oxidative addition of diphenyl diselenide to the non-luminescent Pt(II) precursors [Pt(N[∞]N)(Me)₂], N[∞]N = (bpy, **1a**), (phen, **2a**), (Me₂bpy, **3a**), to give the luminescent Pt(IV) complexes **1b–3b**. The UV-vis absorption spectra of **1b–3b** are characterised by intense bands in the range 240–330 nm. We assigned them to transitions of essentially π–π* character with small metal and PhSe[−] ligand contributions with the help of TD-DFT (time-dependent density functional theory) calculations. The weak long-wavelength bands in the range 350–475 nm are of mixed ligand-to-metal charge transfer (LMCT) (n_(Se)→d_(Pt)/intra-ligand charge transfer (ILCT) (n_(Se)→π*_(Ph) or π_(Ph)→π*_(Ph))/ligand-to-ligand' charge transfer (LLCT) (L = N[∞]N, L' = PhSe[−], M = Pt and n = lone pair) character. The Pt(IV) complexes showed broad emission bands in the solid state at 298 and 77 K, peaking at 560–595 nm with a blue shift upon cooling. Structured emission bands were obtained in the range 450–600 nm, with the maxima depending on the N[∞]N ligands and the solvent polarity (CH₂Cl₂ vs. dimethyl sulfoxide (DMSO) and aqueous tris(hydroxymethyl)aminomethane hydrochloride (*tris*-HCl) buffer). The emissions originate from essentially ligand-centred triplet states (³LC) with mixed ILCT/LMCT contributions as concluded from the DFT calculation. Such dominating PhSe contributions to the emissive states are unprecedented in the world of luminescent diimine-Pt(IV) complexes.

Keywords: OrganoPt(IV); diimine ligands; phenyl selenide; photoluminescence; TD-DFT calculations



check for updates

Citation: Aseman, M.D.; Aghakhanpour, R.B.; Sharifioliaei, Z.; Klein, A.; Nabavizadeh, S.M. Luminescent Diimine-Pt(IV) Complexes with Axial Phenyl Selenide Ligands. *Inorganics* **2023**, *11*, 387. <https://doi.org/10.3390/inorganics11100387>

Academic Editor: Wolfgang Linert

Received: 3 July 2023

Revised: 17 September 2023

Accepted: 23 September 2023

Published: 28 September 2023



Copyright: © 2023 by the authors. Licensee MDPI, Basel, Switzerland. This article is an open access article distributed under the terms and conditions of the Creative Commons Attribution (CC BY) license (<https://creativecommons.org/licenses/by/4.0/>).

1. Introduction

The photophysical properties of heavy transition metal complexes have been of great interest in recent years due to their wide applicability in electroluminescent materials [1–6], in photovoltaic devices [2,5,6], for optical sensing [7,8], as photocatalysts [9–12], in photodynamic therapy [13,14], and as probes for bioimaging [13–18]. Most of the studies focused on the d⁸ systems Au(III) [12,19] and Pt(II) [1,2,4,19,20] and on the d⁶ configured Ir(III), Ru(II), and Os(II) complexes [2,14–18,21,22], which all contain cyclometalated heteroaromatic ligands because they provide widely tunable emission energies and high quantum yields from admixture of triplet ligand-centred (³LC) states to the emitting triplet metal-to-ligand (³MLCT) or ligand-to-metal (³LMCT) excited states [2–4,15,19–24].

In contrast, studies on the optical properties of d^6 -configured cyclometalated Pt(IV) complexes have gained less attention [23–26]. The general low thermal and photo-stability of Pt(IV) complexes that may result in photoisomerisation or reduction in Pt(II) is the main drawback [23,24]. However, the presence of six coordination sites in Pt(IV) complexes offers opportunities for more ligand combinations compared with the four-coordinated Pt(II) complexes. The first luminescent cyclometalated Pt(IV) complexes [Pt(C^N)₂(R)Cl] (R = CH₂Cl, CHCl₂, C^N = 2-thienylpyridine (thpy) or 2-phenylpyridine (ppy)) were reported by Balzani and von Zelewsky in 1986 [26]. Their emission originates from ligand-centered (³LC) states of the cyclometalating ligand with photoluminescence quantum yields in the range 0.05–0.15 in CH₂Cl₂ solution at 293 K. In recent years, additional neutral [Pt(C^N)₂ × 2] complexes containing two anionic ligands X (or R) have been reported [23,24,26–32] and supplemented with cationic derivatives [Pt(C^N)₃]⁺ containing three cyclometalated C^N ligands [23,24,33–38], comparable to the important class of Ir(III) emitters [Ir(C^N)₃] [2,14,16,21,22]. These reports include variations in C^N ligands such as substituted phenyl-pyridines, benzoquinolines, or related heteroaromatic systems [23–35]. Cyclometalating C^C carbene [39] and C^C biphenyl ligands [40] have also recently been introduced. Slightly different structures show the luminescent Pt(IV) complex [Pt(L)Cl₂] with a tetradentate doubly cyclometalated C^N-N^C ligand L [41] and the [Pt(C^N)(S₂Ph)₂][−] complexes containing phenyl dithiolate ligands (S₂Ph^{2−}) [42]. Although these Pt(IV) complexes emit essentially from ligand-centered ³LC states, the simpler complex [Pt(C^N)Cl₃(SMe₂)] (C^N = 2-(4-NMe₂)benzothiazole) was reported to be non-emissive [43].

In contrast, photoluminescent Pt(IV) complexes bearing α -diimine (N^N) bidentate donor ligands are scarce, although the rich photochemistry [44–52] and the basic photo-physics [25,47,48,52–55] of such complexes have been studied in some detail, including the photodecomposition of the Pt(IV)-terpy complexes [Pt(terpy)X₃]⁺ (X = Cl or Br) [53] and the rather historic example of the luminescent [Pt(bpy)(Me)₃I] [25]. A very interesting example of photoreactivity is the photooxidation of the thiophenolate complexes [Pt(N^N)(Me)₃(S-C₆H₄-R)] (N^N = 2,2'-bipyridine (bpy) and derivatives [−]S-C₆H₄-R = thiophenolate) to the sulfinate derivatives [Pt(N^N)(Me)₃(SO₂-C₆H₄-R)] [44,52]. Density functional theory (DFT) calculations showed that emission of the sulfinate complexes originates from the excited state that is formed upon excitation of electrons from Pt–S and Pt–C (*trans* to S) σ bonding orbitals to π^* orbitals of N^N or the aromatic ring of the sulfinate ligands ($\sigma \rightarrow \pi^*$) [44,52], which has also frequently been called sigma(σ)-bond-to-ligand charge transfer (SBLCT) [47,55].

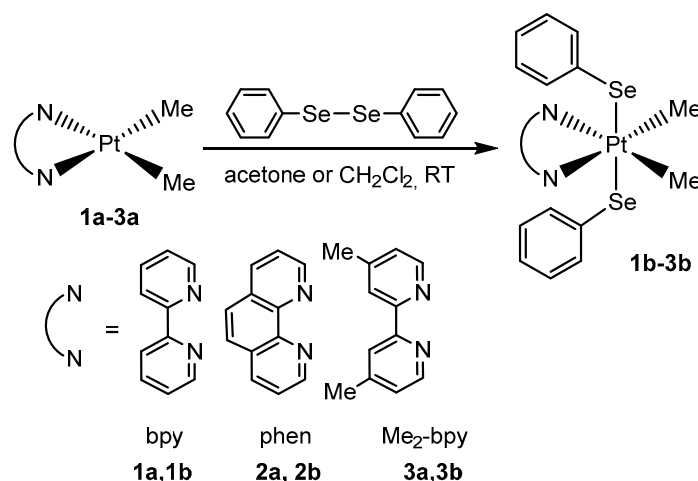
Aiming to extend the structural motifs of photoluminescent diimine Pt(IV) complexes, we stepped over the previously reported complexes [Pt(N^N)(Me)₂(PhE)₂] (E = S or Se) containing heteroaromatic diimines like bpy and its derivatives [56–60]. Herein we report on the preparation of a series of Pt(IV) complexes [Pt(N^N)(Me)₂(PhSe)₂], N^N = bpy (**1b**), phen (**2b**), and Me₂bpy (**3b**), through oxidative addition reaction of diphenyl diselenide to Pt(II) precursors and the study of their UV-vis absorption and photoluminescence (PL). The synthesis and structures of complexes **1b** and **2b** have been previously reported; we were able to add the derivative **3b** to this series. Importantly, the photophysics of the three complexes has not been reported. In parallel to the experiments, we carried out time-dependent DFT (TD-DFT) calculations on the B3LYP level of theory with LANL2DZ basis sets for Pt and Se, and 6-31G(d) basis sets for C, H, and N to probe the nature of the electronic transitions and excited states.

2. Results and Discussion

2.1. Synthesis, Analytical, and Structural Characterisation

The complexes [Pt(N^N)(Me)₂(PhSe)₂], N^N = 2,2'-bipyridine (bpy, **1b**), 1,10-phenanthroline (phen, **2b**), and 4,4'-dimethyl-2,2'-bipyridine (Me₂bpy, **3b**), PhSe[−] = phenyl selenide were synthesised through an oxidative addition reaction of the Pt(II) precursor complexes [Pt(N^N)(Me)₂], **1a–3a**, carrying N^N = bpy (**1a**), phen (**2a**), or Me₂bpy (**3a**) with diphenyl diselenide (Se₂Ph₂) (Scheme 1; For details, see the Methods and Materials

Section) producing pure products that are stable in organic solvents such as CH_2Cl_2 , CHCl_3 , and dimethyl sulfoxide (DMSO) in the absence of light for at least one hour. Extensive visible light irradiation led to decomposition within hours. Although we did not go into the details, we assumed that this is similar to the photoreactivity that has been reported for the thiophenolate complexes $[\text{Pt}(\text{N}^{\wedge}\text{N})(\text{Me})_3(\text{S}-\text{C}_6\text{H}_4-\text{R})]$ [44,52] and the comparable Re(I) thiolate complexes $[\text{Re}(\text{N}^{\wedge}\text{N}')(\text{CO})_3(\text{SR})]$ ($\text{N}^{\wedge}\text{N}' = 1\text{-C}_{12}\text{H}_{25}\text{-1,2,3-triazole-4-(2-pyridyl)}$ (Pyta) or $4\text{-C}_{12}\text{H}_{25}\text{-1,2,3-triazole-1-(2-pyridyl)}$ (Tapy); $\text{R} = 4\text{-X-C}_6\text{H}_4$, $\text{X} = \text{OMe}$, COOMe and NO_2) [61].



Scheme 1. Synthesis routes for complexes **1b–3b**.

Complexes **1b** and **2b** have previously been prepared in a similar manner [58,59] (Figures S1 and S2 in the Supplementary Material). The three complexes were analysed and their structures confirmed using ^1H , $^{13}\text{C}\{^1\text{H}\}$, and $^{77}\text{Se}\{^1\text{H}\}$ NMR spectroscopy (Figures S1–S5).

We optimised the geometry of the S_0 ground states using DFT methods in both the gas phase (Figures 1 and S6–S8) and CH_2Cl_2 solution, with only marginal differences (Tables S1, S3 and S4).

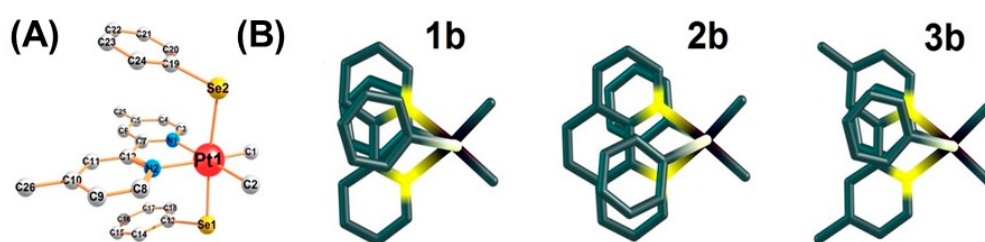


Figure 1. View of the DFT-optimised S_0 structure of **3b** in the gas phase, with atom numbering (A) and top views of **1b**, **2b**, and **3b** (B).

The DFT-calculated **1b** and **2b** structures agree with previously reported experimental structures from single X-ray diffraction (Tables S1 and S3) [58,59]. They show that both PhSe planes point towards the $\text{N}^{\wedge}\text{N}$ ligand plane (Figure 1A) but co-planarity is prevented through the Pt–Se–C angles of about 105° and Se–Pt–Se angles of about 174° , deviating from the ideal 180° . The most important difference between the phen complex **2b** and the bpy complexes **1b** and **3b** is the intramolecular stacking motif of the PhSe phenyl group with the aromatic system in the diimines (Figure 1). This corresponds with differences in the dihedral angles between the two PhSe planes, which are relatively small for the bpy and Me_2bpy complexes (about $6\text{--}9^\circ$, independent of the medium) but large for the phen derivative **2b** with about 51° in the gas phase calculations and about 20° in CH_2Cl_2 .

Based on the DFT-optimised **1b–3b** structures in CH_2Cl_2 , the energies and composition of the molecular orbitals (MOs) of the complexes were calculated (Figures 2 and S11–S13, Tables S5–S7). The gaps between the highest occupied and the lowest unoccupied molecular orbitals (HOMO–LUMO gaps) increase along the series **1b** (3.109 eV) < **2b** (3.135 eV) < **3b** (3.169 eV), reflecting the increased electron density through the additional C=C group in the backbone of phen and the Me substitutes compared with bpy. The occupied MOs are distributed over the PhSe^- ligands, with HOMO–HOMO-2 localised at the Se lone-pairs (~85%) with no difference for **1b–3b**, while HOMO-3–HOMO-5 orbitals are centered on the phenyl cores. Unoccupied MOs are mainly localised on the N^N chelate ligands (92 to 99%), again with only minor differences for series **1b–3b**. HOMO had small Pt contributions (~14%) with a d_{xy} character for LUMO+1 (d_{z^2}), although the latter is better described as $\sigma\text{-Se–Pt}$ contribution (Figure S11). For LUMO+4, a mixed Pt $d_{x^2-y^2}/\sigma\text{ Pt–CH}_3$ character is observed (~70%) for **1b** and **3b**. For complex **2b**, both contributions were also found, although the labelling was different (LUMO+2 and LUMO+5). The energies of these two orbitals are different (~1.8 eV), pointing to a distortion of the octahedral symmetry with the empty d_{z^2} and $d_{x^2-y^2}$ not degenerating.

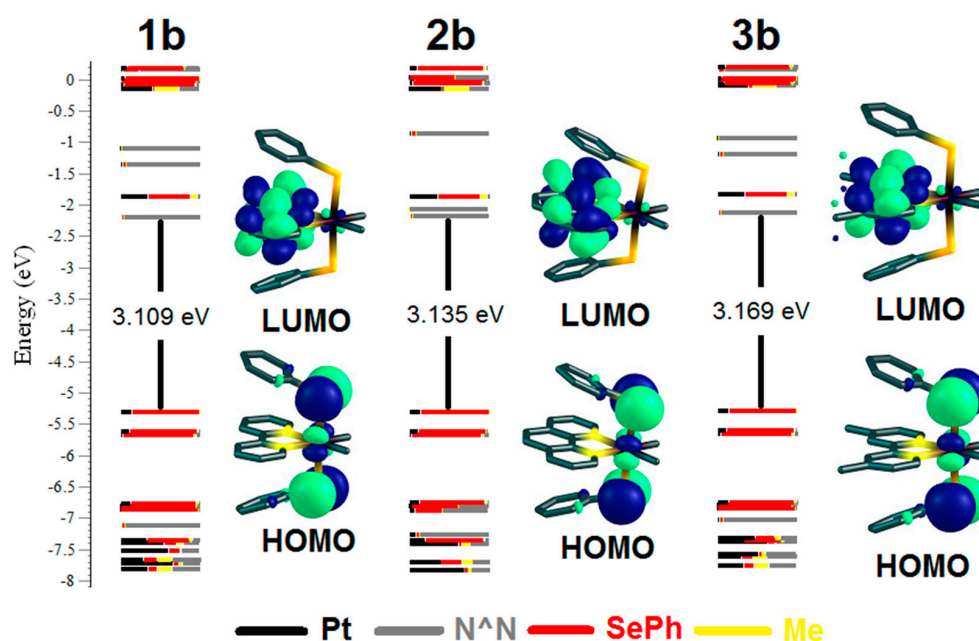


Figure 2. Energy level diagrams and composition of the highest occupied molecular orbital (HOMO) and the lowest unoccupied molecular orbital (LUMO) for **1b–3b**.

2.2. UV-Vis Absorption Spectra and TD-DFT Calculations

The experimental UV-vis absorption spectra of compounds **1b–3b** in CH_2Cl_2 solution are very similar (Figures 3 and S9), with two intense maxima at 240 and 320 nm. The phen complex **2b** has an additional band at 274 nm. These UV bands can be provisionally assigned to $\pi-\pi^*$ transitions in the N^N ligands. Possible admixtures can include intra-ligand $\text{IL}'_{(\text{PhSe})}$ charge transfer ($\text{IL}'\text{CT}$), metal-to-ligand $_{(\text{N}^{\text{N}})}$ charge transfer (MLCT), ligand $'_{(\text{PhSe})}$ -to-ligand $_{(\text{N}^{\text{N}})}$ charge transfer ($\text{L}'\text{LCT}$), and ligand'-to-metal charge transfer ($\text{L}'\text{MCT}$) character. Additional weak absorptions were observed in the range 350–475 nm as shoulders that are provisionally assigned to $\text{L}'\text{LCT}$ transitions with small MLCT and $\text{L}'\text{MCT}$ contributions in line with the ground state frontier orbitals (Figure 2).

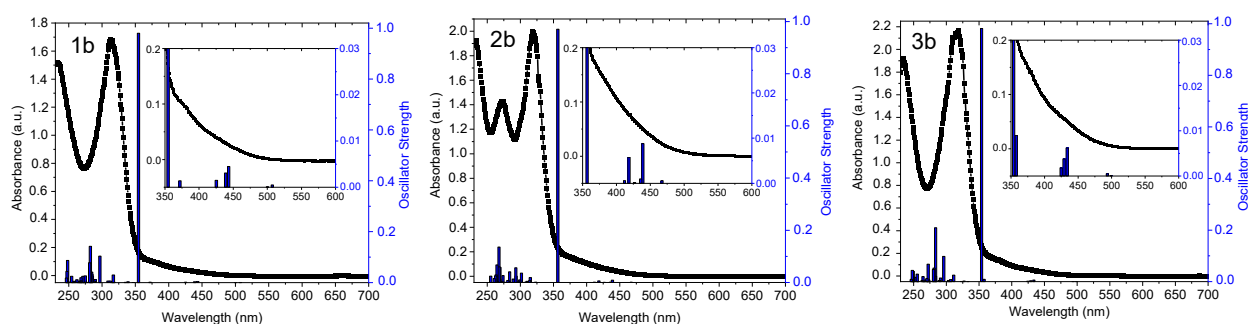


Figure 3. Experimental UV-vis absorption spectra (black spectra in CH_2Cl_2) and TD-DFT-calculated transitions as blue bars for **1b**, **2b**, and **3b**.

For future use in biological media, we also dissolved and studied the complexes in aqueous *tris*(hydroxymethyl)aminomethane hydrochloride (*tris*-HCl) buffer with the help of small amounts of DMSO as a co-solvent. The same absorptions were found in the *tris*-HCl buffer solution. After standing for 30 min in the dark, the long wavelength absorptions were slightly decreased, while UV absorptions remained stable (Figure S10). This is probably due to slow hydrolysis under these conditions adding potential instability to the slow photodecomposition in the presence of light.

The TD-DFT-calculated transitions match the experimental spectra in that they qualitatively reproduce the differences between the bpy complexes **1b** and **3b**, in contrast to the phen complex **2b**, while the calculated maxima are generally red-shifted compared with the experimental maxima (for data, see Tables S8–S10). For the bpy complex **1b**, the long wavelength region between 300 and 500 nm includes several excited states (S_1 to S_6) with very small oscillator strengths in keeping with the weak absorptions observed in this range (Figure 3, inset). They are assigned to transitions with mixed L'LCT/MLCT or L'MCT/IL'CT character, with L' representing the PhSe ligands and IL'CT describing charge transfer from Se $n_{(\text{Se})}$ lone pairs (or p orbitals) to π^* orbitals of the Ph group (Table S8). The HOMO \rightarrow LUMO transition for **1b** has mixed L'LCT ($n_{(\text{Se})} \rightarrow \pi^*_{(\text{bpy})}$)/MLCT ($d_{(\text{Pt})} \rightarrow \pi^*_{(\text{bpy})}$) character in which the most important contribution form, the PhSe ligand, comes from the lone-pairs, n, on the Se atom. In contrast to this, the HOMO \rightarrow L+1 transition has a mixed L'MCT/IL'CT ($n_{(\text{Se})} \rightarrow \pi^*_{(\text{Ph})}$) character. The $S_0 \rightarrow S_7$ transition (H-1 \rightarrow L+1, 354 nm) has the highest oscillator strength (0.9801) and mixed L'MCT/IL'CT character. Similar transitions with similar characters were calculated for the Me_2bpy complex, **3b**. They are all slightly blue-shifted (Table S9) in keeping with the electron-releasing character of the Me substituents on the bpy core. Despite some very small contributions to LUMO+4 in **1b** and **3b**, the Me ligands show overall negligible contributions. For the phen complex, **2b**, the long wavelength region shows eight excited states of low energy (S_1 – S_8), with energies slightly blue-shifted compared to **1b**; both findings are in line with the additional C=C group in the phen backbone.

When comparing the results of our calculations with those previously reported for complexes $[\text{Pt}(\text{bpy})(\text{Me})_3(\text{SR})]$ ($\text{R} = \text{H}$ or $p\text{-CO}_2\text{C}_6\text{H}_4$) [50] and $[\text{Pt}(\text{bpy})(\text{Me})_3(\text{SO}_2\text{-C}_6\text{H}_4\text{-R})]$ ($\text{SO}_2\text{-C}_6\text{H}_4\text{-R} = p\text{-R-phenyl-sulfonates}$, $\text{R} = \text{H}$ or NO_2) [52], we found a role for our PhSe^- ligands that was similar to that of S-aryl ligands contributing both the S lone pairs and the aryl π^* system to electronic transitions. Moreover, the $\sigma \rightarrow \pi^*$ transitions involving the Pt–S and Pt–C (*trans* to S) in these systems are similar to the $\sigma \rightarrow \pi^*$ contributions from the PhSe^- ligands in our systems. On the other hand, the intramolecular stacking of the PhSe^- and N^N ligands that characterise our structures have been found for $[\text{Pt}(\text{bpy})(\text{Me})_3(\text{SO}_2\text{-Ph})]$ but not for $[\text{Pt}(\text{bpy})(\text{Me})_3(\text{S-C}_6\text{H}_4\text{-CO}_2)]$ or $[\text{Pt}(\text{bpy})(\text{Me})_3(\text{SO}_2\text{-C}_6\text{H}_4\text{-NO}_2)]$ [52]. In the above-mentioned $\text{Pt}(\text{Me})_3$ complexes, as well as in the $[\text{Pt}(\text{N}^{\wedge}\text{N})(\text{Me})_3\text{I}]$ [48,54,55], $[\text{Pt}(\text{N}^{\wedge}\text{N})(\text{Me})_4]$ [47,48,55], and $[\text{Pt}(\text{N}^{\wedge}\text{N})(\text{Me})_2(\text{SnPh}_3)_2]$ derivatives [55], the axial Me ligands do not contribute to the long wavelength transitions.

Similar to the Pt(IV) complexes, the intense absorptions at around 330–355 nm observed for the Re(I) thiolate complexes $[\text{Re}(\text{N}^{\wedge}\text{N}')(\text{CO})_3(\text{SR})]$ ($\text{N}^{\wedge}\text{N}' = \text{pyridyl-trizoles}$) are

assigned to predominantly π - π^* transitions with admixtures of LL'CT (thiolate to N^N) and MLCT (Re to N^N) character. Weak bands were observed at lower energies and DFT calculations suggest L'CT and L'MCT (thiolate to Re) character [61].

2.3. Photoluminescence Spectroscopy

Complexes **1b**–**3b** emit yellow to orange light in different media at ambient temperatures when irradiated at 365 nm (Figures 4 and 5), in stark contrast to their corresponding deeply red-coloured Pt(II) precursors [Pt(N^N)(Me)₂], **1a**–**3a**, which are non-emissive under the same conditions [62]. Changing the excitation wavelength within the range 300–400 nm had no marked impact on the shape or maxima of the emission bands.

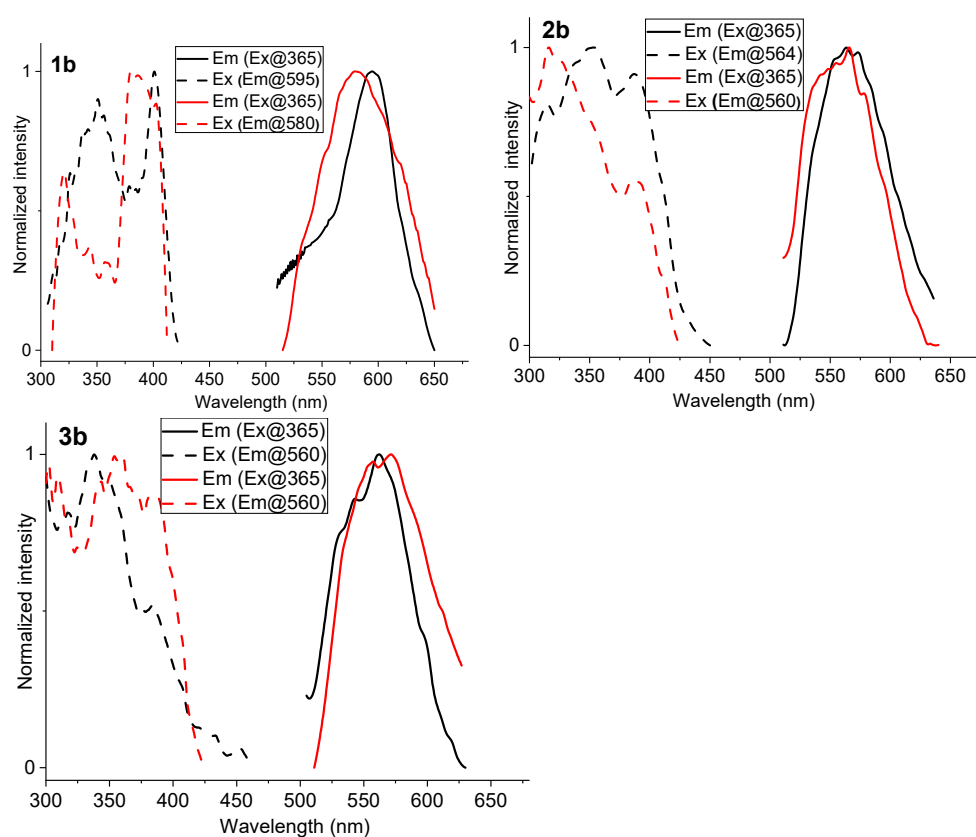


Figure 4. Photoluminescence (solid lines) and excitation (dashed lines) spectra of **1b**, **2b**, and **3b** in the solid state at 298 K (black lines) and 77 K (red lines).

In the solid state, the emission spectra for **1b**–**3b** had broad bands with maxima between 554 and 595 nm (Figure 4, Table 1). Different temperatures (298 vs. 77 K) did not make a marked difference. At 298 K, the highest photoluminescence quantum yield (Φ_L) was 0.081 for **2b**, while **1b** and **3b** had slightly lower values of 0.069 and 0.065, respectively. At 77 K, the Φ_L value for **2b** increased and reached 0.14. The excitation spectra showed intense maxima in the range 300–400 nm, with the most red-shifted maximum observed for **1b**.

More structured emission bands were observed in the CH₂Cl₂ solution, with their maxima blue-shifted compared with the solids (Figure 5, Table 1). Within our series of complexes, the energy of the emission maximum increased for **2b** and **3b** compared with **1b**. The excitation spectra showed sharp bands at around 360 nm for all three complexes. This means a Stokes Shift of about 8400 cm⁻¹ for **1b** and about 7400 cm⁻¹ for **2b** and **3b**. This is consistent with a triplet character of the excited states, thus a triplet emission. The most intense excitation bands at around 360 nm are markedly red-shifted compared with the intense absorption bands observed at around 320 nm. The energy difference of about 3500 cm⁻¹ suggests that the most intensely absorbing state is not identical to the state

responsible for the emission. Unfortunately, the Φ_L values are generally very low in the CH_2Cl_2 solution (0.002–0.006) and the PL spectra for **1b** differ from those for **2b** and **3b**. Therefore, we cannot rule out the effect of different species or impurities on PL behaviour.

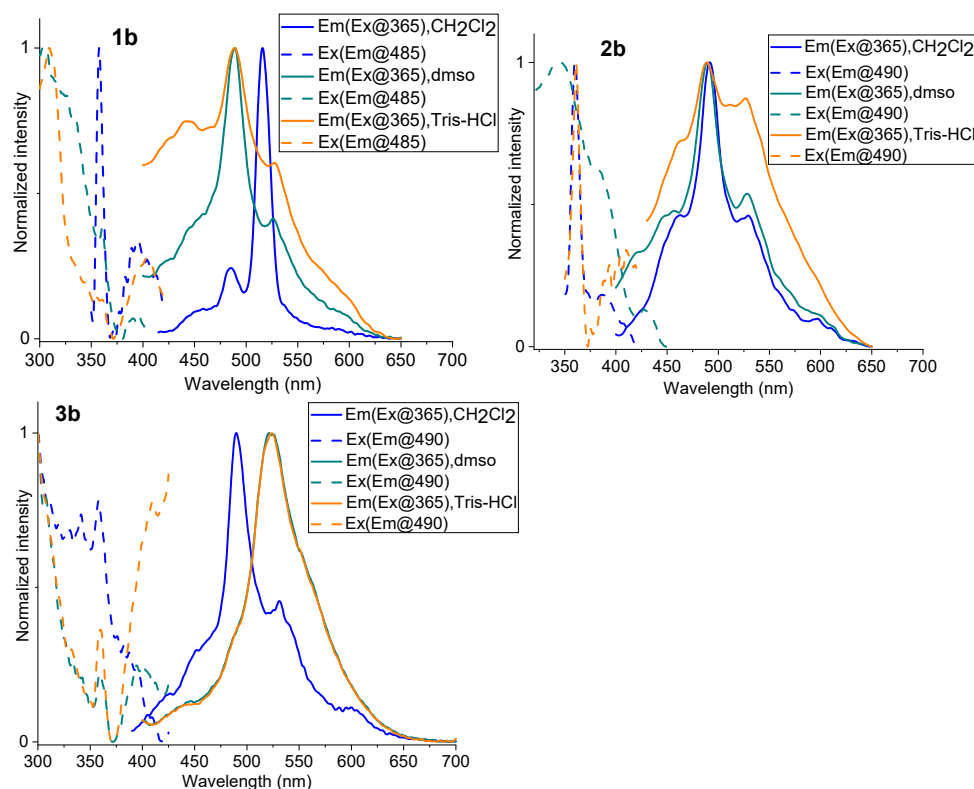


Figure 5. Photoluminescence (solid lines) and excitation (dashed lines) spectra for **1b**, **2b**, and **3b** in CH_2Cl_2 (blue lines), DMSO (green lines), and *tris*-HCl (orange lines) solutions at 298 K.

Table 1. UV-vis absorption and emission data for Pt(IV) complexes ^a.

Complex	$\lambda_{\text{abs}}/\text{nm}$ ($10^5 \epsilon/\text{M}^{-1} \text{cm}^{-1}$)	State (T)	$\lambda_{\text{em}}/\text{nm}$	Φ_L
1b	400 (0.0595), 313 (1.697)	solid (298 K)	<u>595</u>	0.069
		solid (77 K)	<u>580</u>	0.117
		CH_2Cl_2 (298 K)	453, <u>484</u> , <u>516</u>	0.0065
		DMSO (298 K)	450, <u>484</u> , <u>526</u>	0.0123
		<i>tris</i> -HCl (298 K)	442, <u>484</u> , <u>526</u>	0.0093
		solid (298 K)	<u>564</u>	0.081
2b	400 (0.1167), 318 (2.003), 272 (1.451)	solid (77 K)	<u>560</u>	0.140
		CH_2Cl_2 (298 K)	463, <u>490</u> , <u>529</u>	0.0017
		DMSO (298 K)	456, <u>490</u> , <u>528</u>	0.0032
		<i>tris</i> -HCl (298 K)	462, <u>490</u> , <u>526</u>	0.0090
		solid (298 K)	<u>560</u>	0.065
		solid (77 K)	<u>560</u>	0.101
3b	400 (0.1004), 314 (2.184)	CH_2Cl_2 (298 K)	453, <u>490</u> , <u>530</u>	0.0042
		DMSO (298 K)	447, <u>486</u> , <u>522</u>	0.0050
		<i>tris</i> -HCl (298 K)	447, <u>486</u> , <u>522</u>	0.0053

^a Excitation wavelength $\lambda_{\text{exc}} = 365 \text{ nm}$ in all cases. The absorption spectra were obtained in CH_2Cl_2 . Emission spectra in Ar-purged CH_2Cl_2 solution, $c = 10^{-5} \text{ M}$, emission maxima are underlined. *tris*-HCl = aqueous *tris*-HCl buffer (pH = 7.4), for Ar-purged DMSO and *tris*-HCl solutions $c = 0.01 \text{ M}$. Φ_L = photoluminescence quantum yields.

To probe for the influence of solvent polarity on the PL of **1b–3b**, we studied DMSO and aqueous *tris*-HCl buffer (pH = 7.4, 0.01 M) solutions in addition to CH_2Cl_2 . A further background is the idea of using these complexes as probes in biological media. As in

the CH₂Cl₂ solution, the complexes were emissive at 298 K and also showed partially structured emission bands (Figure 5). Interestingly, the solvents had almost no impact on the shape and energies of the emission band of the phen complex **2b** (Figure 5), while **1b** showed a red-shifted maximum (516 nm) for the CH₂Cl₂ solution compared with the DMSO and *tris*-HCl buffer solutions (484 nm), and **3b** showed a blue-shifted maximum in CH₂Cl₂ (490 nm) compared with the DMSO and *tris*-HCl buffer solutions (522 nm). The Φ_L values are generally low (0.0017–0.0123) and are higher in each case in the polar media, for **2b** and **3b**, with the highest values found in aqueous *tris*-HCl buffer (Table 1). In the excitation spectra, the intense band observed in CH₂Cl₂ solutions at around 360 nm is also found for **2b** in *tris*-HCl and **3b** in both polar media, but with a markedly lower intensity. Additional broad, blue-shifted bands were found for **1b** in DMSO and *tris*-HCl and for **2b** in DMSO. We assume that both Me substituents on the bpy ligand and the C=C backbone of the phen ligand render the molecules more lipophilic, thus minimising the effect of solvent polarity on the chromophoric parts of the complexes.

Unfortunately, the lifetimes were too short to measure using our equipment in the lab and we assumed that they were in the nanosecond domain. For the Pt(IV) complex [Pt(bpy)(Me)₃(S-C₆H₄-R)]⁻ (S-C₆H₄-R = 4-methoxycarbonylthiophenolate), a triplet emission lifetime of 5.6 ns was reported [52], while for [Pt(Me)₃(bpy)I], 2.8 ns was recorded [52]. The lifetimes of complexes **1b–3b** will be the subject of future studies.

To rationalise the emission spectra, the geometry of the T₁ triplet state for complexes **1b** and **2b** were DFT-optimised in the gas phase. Unfortunately, attempts to do the same for **3b** were unsuccessful. Energy differences between the T₁ and S₀ states representing the theoretical emissions were calculated as 2.146 eV (578 nm) and 2.098 eV (591 nm) for complexes **1b** and **2b**, respectively. These are in very good agreement with the experimental values recorded for **1b** and **2b** at 595 nm and 564 nm in the solid at 298 K (Table 1). Furthermore, the observed red-shift in the main emission component in the CH₂Cl₂ solution from 490 to 515 nm when going from **2b** (phen) to **1b** (bpy) is also qualitatively reproduced, although the total values deviate markedly. This marked deviation is due to the gas phase conditions used for the DFT calculations and is in line with the strong dependence of the emission on the medium found in the experiments.

For complexes **1b** and **2b**, plots of LSOMO (Lowest Singly Occupied Molecular Orbital) and HSOMO (Highest Singly Occupied Molecular Orbital) compositions (Figure 6) showed high similarities between LSOMO and HOMO compositions (Figure 2), while the compositions of HSOMO and LUMO in both complexes were different. LUMO+1 and LUMO+2 levels are stabilised when they are converted to HSOMO for **1b** and **2b**, respectively. LSOMO and HSOMO are mainly located on the Pt and Se atoms (Figure 6). The emissive excited states of **1b** and **2b** can thus be described as having mixed ³IL'CT/³L'MCT characters, with a significant contribution of the PhSe ligands. This is in agreement with the intense excitations observed at around 360 nm where the TD-DFT-calculated transitions show strong IL'CT contributions (Tables S8 and S9). This also accounts for the marked differences between absorptions with large contributions of the N^N ligands to the transitions and the excitations populating triplet excited states with essential PhSe and Pt characters and supports our assumptions of different absorption and excitation characters.

Broad, unstructured emission bands were reported for complexes [Pt(N^N)(Me)₃(SR)] (N^N = bpy or 4,4'-(CO₂Me)₂bpy; R = *p*-CO₂C₆H₄) [51] and [Pt(N^N)(Me)₃(SO₂-C₆H₄-R)] (N^N = bpy, phen, 4,7-Ph₂phen and dppz (dipyrido[3,2-*a*:2',3'-*c*]phenazine); SO₂-C₆H₄-R = *p*-R-phenyl-sulfonates, R = H, CO₂Me, OMe, or NO₂) [52], although they had similar energies as our complexes. The same is true for [Pt(bpy)(Me)₃I], which emits at 528 nm in EtOH at 298 K [25]. Similar emissions were found for the related Re(I) thiolate complexes [Re(N^N')(CO)₃(SR)] and a mixed ³MLCT/³L'LCT character was concluded from DFT calculations [61].

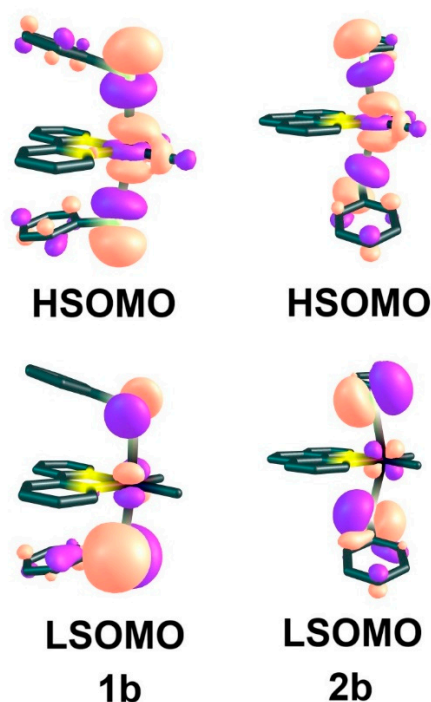


Figure 6. DFT-calculated HSOMO and LSOMO compositions of complexes **1b** and **2b**.

For $[\text{Pt}(i\text{Pr-DAB})(\text{Me})_3\text{I}]$, a broad emission band was recorded at 550 nm in glassy frozen 2-Me-THF at 90 K, while for the tetramethyl Pt(IV) complexes $[\text{Pt}(\text{N}^{\wedge}\text{N})(\text{Me})_4]$ with $\text{N}^{\wedge}\text{N} = \text{tmphen}$ (3,4,7,8-tetramethylphenanthroline) or *iPr-DAB* (1,2-di(isopropyl)diazabuta diene), broad emission bands were observed at 775 nm (*iPr-DAB*) and 600 nm (tmphen) [55]. Quantum chemical calculations for the $(\text{Me})_3\text{I}$ complexes showed a ${}^3\text{XLCT}$ character for the emission ($X = \text{I}$) similar to the $\text{L}'\text{LCT}$ contribution for thiolate complexes [51], while for the $(\text{Me})_4$ derivatives, an SBLCT character of the emission was concluded [55]. This is supported by the markedly red-shifted emission of complex $[\text{Pt}(i\text{Pr-DAB})(\text{Me})_2(\text{SnPh}_3)_2]$ to 809 nm in line with the reduced axial Sn–Pt bond strength and σ -donating power of SnPh_3 compared with Me. The $(\text{Me})_4$ complexes and the $(\text{Me})_2(\text{SnPh}_3)_2$ derivative were photo-reactive at ambient temperatures, forming the Pt(II) species [55].

Structured emission bands were observed at 298 K in CH_2Cl_2 solutions and PMMA matrices for cyclometalated Pt(IV) complexes *fac*- $[\text{Pt}(\text{C}^{\wedge}\text{N})_2(\text{C}_6\text{F}_5)\text{Cl}]$ with $\text{C}^{\wedge}\text{N} = \text{bzq}$ (benzoquinoliny), dfppy (2-(2,4-difluorophenyl)pyridyl), pq (2-phenylquinoliny), thpy (2-thienylpyridyl), pbt (2-phenylbenzothiazole), or Br-pbt (2-(4-bromophenyl)benzothiazole) and *mer*- $[\text{Pt}(\text{C}^{\wedge}\text{N})_2(\text{C}_6\text{F}_5)(\text{CN})]$ ($\text{C}^{\wedge}\text{N} = \text{pbt}, \text{Br-pbt}$) [31]. Additionally, the complex $[\text{Pt}(\text{thpy})(\text{tpy})(\text{Cl})_2]$ [32] and several derivatives of $[\text{Pt}(\text{C}^{\wedge}\text{N})(\text{C}^{\wedge}\text{N}')(\text{Cl})_2]$ [36] containing two different cyclometalating $\text{C}^{\wedge}\text{N}$ ligands, including $[\text{Pt}(\text{C}^{\wedge}\text{N})(\text{C}^{\wedge}\text{C}_{\text{carbene}})(\text{Cl})_2]$ [39], and the series of complexes $[\text{Pt}(\text{C}^{\wedge}\text{N})_2(\text{Me})\text{Cl}]$ ($\text{C}^{\wedge}\text{N} = \text{ppy}, \text{dfppy}, \text{thpy}$ and more) [29] showed structured emission bands in CH_2Cl_2 solution at 298 K. The bands are very similar, in both structure and energy, to what we found for our complexes. The structure is in keeping with the essential ${}^3\text{LC}$ character of the emission of these cyclometalate complexes. TD-DFT calculations of the electronic transitions support ${}^3\text{MLCT}$ and ${}^3\text{LMCT}$ admixtures to the ${}^3\text{LC}$ emissive states for the $[\text{Pt}(\text{C}^{\wedge}\text{N})_2(\text{C}_6\text{F}_5)\text{Cl}]$ complexes [31], while small to negligible LMCT contributions were found for $[\text{Pt}(\text{C}^{\wedge}\text{N})(\text{C}^{\wedge}\text{N}')(\text{Cl})_2]$ derivatives [29,32,39].

We found, for our previously unreported $[\text{Pt}(\text{N}^{\wedge}\text{N})(\text{Me})_2(\text{PhSe})_2]$ systems, a predominant PhSe ligand-character in the triplet excited states, with mixed ${}^3\text{IL}'\text{CT}/{}^3\text{LMCT}$ contributions being responsible for the pronounced structuring and efficient emission in solution at 298 K. This contrasts with the TD-DFT-calculated absorption spectra showing appreciable contributions of the $\text{N}^{\wedge}\text{N}$ chelate ligands with mixed $\text{L}'\text{LCT}/\text{MLCT}$ contributions in addition to the ${}^3\text{IL}'\text{CT}/{}^3\text{LMCT}$, and also differs from previously reported Pt(IV) systems

with Pt(N \bar{N}) or Pt(C \bar{N}) scaffolds, for which essential contributions from the N \bar{N} or C \bar{N} chelate ligands (L \bar{L} CT or MLCT) to the emissive states were reported. We ascribe this to a perfect match between the axial PhSe ligands and the Pt orbitals in terms of energy and orbital overlap.

3. Methods and Materials

3.1. General Procedures and Materials

^1H NMR, $^{13}\text{C}\{^1\text{H}\}$ NMR, and $^{77}\text{Se}\{^1\text{H}\}$ spectra were obtained using a Bruker Avance (400 MHz) instrument at 298 K. The chemical shifts (δ) are reported in ppm relative to their external standards (SiMe_4 for ^1H and ^{13}C , Ph_2Se for ^{77}Se), and the coupling constant J is expressed in Hz. UV-vis absorption spectra were recorded using a PerkinElmer Lambda 25 spectrophotometer. Luminescence spectra were measured at 298 and 77 K using a PerkinElmer LS45 fluorescence spectrometer. CH_2Cl_2 , DMSO, and aqueous *tris*-HCl buffer solutions were Ar-purged prior to use. Due to the virtual insolubility of the complexes in the *tris*-HCl buffer solution, small amounts of DMSO were added. Absolute photoluminescence quantum yields in the solid state were measured using an integrating sphere. Quantum yields in solution were measured using MeCN solutions of complex $[\text{Ru}(\text{bpy})_3](\text{PF}_6)_2$ as standard [63].

2,2'-bipyridine (bpy), 1,10-phenanthroline (phen), 4,4'-dimethyl-2,2'-bipyridine (Me_2bpy), diphenyl diselenide (Se_2Ph_2), and *tris*(hydroxymethyl)aminomethane (*tris*-HCl) were obtained from Sigma-Aldrich (Merck, Darmstadt, Germany) and used without further purification. Reactions were performed in solvents purified and dried according to standard procedures [64]. Complexes $[\text{Pt}(\text{bpy})(\text{Me})_2(\text{PhSe})_2]$ (**1b**) [58] and $[\text{Pt}(\text{phen})(\text{Me})_2(\text{PhSe})_2]$ (**2b**) [59] were prepared and analysed as described in the literature.

3.2. Synthesis of $[\text{Pt}(\text{Me}_2\text{bpy})(\text{Me})_2(\text{PhSe})_2]$ **3b**

A total of 38.1 mg Se_2Ph_2 (0.122 mmol) was added to a solution of 50 mg $[\text{Pt}(\text{Me}_2\text{bpy})(\text{Me})_2]$ (0.122 mmol) in 20 mL CH_2Cl_2 , and the yellow solution stirred for 1 h. The solvent was evaporated and the resulting pale-yellow solid was washed with diethyl ether (3×3 mL) and dried under an air atmosphere. Yield: 79%. Elem. Anal. Calcd. for $\text{C}_{26}\text{H}_{28}\text{N}_2\text{PtSe}_2$ ($M_W = 721.51$ g.mol $^{-1}$): C, 43.28; H, 3.91; N, 3.88; Found: C, 43.01 H, 3.54 N, 3.91. ^1H NMR in CDCl_3 : δ (^1H) 1.55 (s, $^3J_{\text{PtH}} = 70.3$ Hz, 6H, Me ligands), 2.44 (s, 6H, Me_2bpy), 6.48 (dd, $^3J_{\text{HH}} = 7.3$ Hz, $^3J_{\text{HH}} = 7.3$ Hz, 4H, H^m PhSe), 6.67 (d, $^3J_{\text{HH}} = 7.0$ Hz, 1H, H^o PhSe), 6.83 (t, $^3J_{\text{HH}} = 6.9$ Hz, 2H, H^p PhSe), 7.12 (d, $^3J_{\text{HH}} = 5.1$ Hz, 2H, H^5 Me_2bpy), 7.30 (s, 2H, H^3 Me_2bpy), 8.41 (d, $^3J_{\text{PtH}} = 15.5$ Hz, $^3J_{\text{HH}} = 5.8$ Hz, 2H, H^4 Me_2bpy); ^{13}C NMR in CDCl_3 : δ ($^{13}\text{C}\{\text{H}\}$) -6.99 (s, $^1J_{\text{PtC}} = 595$ Hz, 2C, Me ligands), 21.17 (s, 2C, Me substituents Me_2bpy), 123.01 (s, $^3J_{\text{PtC}} = 9.9$ Hz, 2C, C^5 Me_2bpy), 124.91 (s, $^3J_{\text{PtC}} = 7.7$ Hz, 2C, C^3 Me_2bpy), 126.76 (s, $^2J_{\text{PtC}} = 16.1$ Hz, 2C, C^2 Me_2bpy), 126.99 (s, $^3J_{\text{PtC}} = 7.5$ Hz, 4C, C^o PhSe), 130.44 (s, $^2J_{\text{PtC}} = 30.4$ Hz, 2C, C^i PhSe), 137.21 (s, $^4J_{\text{PtC}} = 7.7$ Hz, 4C, C^m of PhSe), 146.08 (s, $^2J_{\text{PtC}} = 13.3$ Hz, 2C, C^6 Me_2bpy), 149.35 (s, 2C, C^p PhSe), 153.37 (s, 2C, C^4 Me_2bpy); ^{77}Se NMR in CDCl_3 : δ ($^{77}\text{Se}\{^1\text{H}\}$) 347.75 (s, $^1J_{\text{PtSe}} = 183.1$ Hz, 2Se).

3.3. Computational Details

DFT calculations were carried out on the B3LYP level of theory [65–67] using the Gaussian09 program suite [68], LANL2DZ basis sets for Pt and Se atoms [69,70], and 6-31G(d) basis sets for C, H, and N atoms. The calculations were run either in the gas phase or CH_2Cl_2 solution using the CPCM (conductor-like polarisable continuum model) model [71,72]. The structures of the electronic S_0 and T_1 states were optimised without any symmetry constraints. The UV-vis absorption spectra were calculated using time-dependent DFT (TD-DFT) methods and emission energies were calculated using DFT-optimised geometries. The composition of molecular orbitals and the TD-DFT bars for electronic transitions were drawn using the “Chemcraft version 1.7” software [73]. Data for the electronic transitions were extracted using the GaussSum software [74].

4. Conclusions

A series of diimine-Pt(IV) complexes $[\text{Pt}(\text{N}^*\text{N})(\text{Me})_2(\text{PhSe})_2]$ with $\text{N}^*\text{N} = 2,2'$ -bipyridine (bpy, **1b**), 1,10-phenanthroline (phen, **2b**), and 4,4'-dimethyl-2,2'-bipyridine (Me_2bpy , **3b**) chelate ligands and axial PhSe^- ligands were found to be luminescent in solid (298 and 77 K) and solution at 298 K and thus formed a new class of luminescent Pt(IV)-diimine complexes. Long wavelength absorptions were observed as shoulders in the range 350–475 nm. Time-dependent density functional theory (TD-DFT) calculations attribute the lowest energy bands (HOMO–LUMO) to transitions with mixed L'LCT ($n_{(\text{Se})} \rightarrow \pi^*_{(\text{bpy})}$)/MLCT ($d_{(\text{Pt})} \rightarrow \pi^*_{(\text{bpy})}$) character, with the most important contribution of the PhSe^- ligand coming from the lone pair (n) on the Se atom. Transitions slightly higher in energy (HOMO→L+1) have mixed L'MCT/IL'CT ($n_{(\text{Se})} \rightarrow \pi^*_{(\text{Ph})}$) character. The 200–350 nm range is dominated by one intense band at around 315 nm. The TD-DFT-calculated energy for this band is approximately 354 nm, thus slightly red-shifted, and the assignment shows essentially π – π^* character of the transitions, with smaller contributions from the PhSe^- ligand (L'LCT and IL'CT) and metal (MLCT). Overall, the TD-DFT-calculated data is in excellent agreement with the experimental data.

Upon irradiation at 365 nm, which is markedly blue-shifted to low-energy absorptions, the maximum of unstructured emission bands of the complexes in the solid ranges lies at 560 nm for **3b**, 564 nm for **2b**, and 595 nm for **1b**, in line with the electron-donating properties of the Me substituents and the additional C=C group in the phen ligand compared with bpy. Structured bands were observed in fluid CH_2Cl_2 solution, but the wavelength dependence of the emission maximum is the same as in the solid, with blue-shifted bands for **2b** and **3b** compared with **1b**. In both the solid and CH_2Cl_2 solution, intense excitation bands were found in the range 300–400 nm, with pronounced maxima at 360 nm in the CH_2Cl_2 solution. The Stokes shift of these sharp excitations and the emission maxima are large (8400 – 7400 cm^{-1}), which strongly supports a triplet character of the emission. However, the luminescence lifetimes are below the μs range and remain to be studied. In the very polar solvents, DMSO and aqueous *tris*-HCl buffer, the emission maximum for **3b** was observed at 522 nm, while those for **1b** and **2b** were blue-shifted ($\sim 490 \text{ nm}$). This is remarkable, as the overall structures of the three complexes are very similar. In future studies, we will add other α -diimine ligands such as the sterically bulky 2,9-dimethyl-phenanthroline (neocuproin) and 6,6'-dimethyl-bipyridine as well as other bpy and phen derivatives with electron-withdrawing substituents.

Using the DFT-optimised T_1 and S_0 geometries for **1b** and **2b**, the $T_1 \rightarrow S_0$ transitions were calculated as 578 nm and 591 nm, respectively, in agreement with the experimental values, 595 nm and 564 nm, recorded in the solid at 298 K. While the LSOMO (Lowest Singly Occupied Molecular Orbital) compositions showed high similarities with the HOMO compositions, the HSOMO and LUMO compositions in **1b** and **2b** differ. LSOMO and HSOMO are mainly located on the Pt and Se atoms and the excited states of **1b** and **2b** can thus be described as having essentially mixed ${}^3\text{IL}'\text{CT}/{}^3\text{L}'\text{MCT}$ character, with a significant contribution of PhSe ligands to the emissive excited states. This is in excellent agreement with the observed intense excitations at around 360 nm, for which TD-DFT-calculated transitions show strong IL'CT contributions and account for the marked differences between absorption and excitation spectra. The triplet character is in line with the observed Stokes shifts, and the structuring is in line with the strong ${}^3\text{LC}$ (= PhSe) character.

While previously reported Pt(IV) systems with Pt(N^*N) or Pt(C^*N) scaffolds show essential contributions of the N^*N or C^*N chelate ligands (L'LCT or MLCT) to the emissive states, our $[\text{Pt}(\text{N}^*\text{N})(\text{Me})_2(\text{PhSe})_2]$ systems reported herein show a predominant PhSe ligand-character for the emissive triplet excited states, with mixed ${}^3\text{IL}'\text{CT}/{}^3\text{L}'\text{MCT}$ contributions. We ascribe this to a perfect match between the axial PhSe ligands and the Pt orbitals in terms of energy and orbital overlap. We will study the impact of substitutions at the axial PhSe on photophysics in the future. We will also add ps time-resolved PL spectroscopy and study the observed photo-sensibility of the compounds in solution in

more detail. Finally, we will explore the potential use of the complexes as luminophores in fluorescent cell imaging.

Supplementary Materials: The following supporting information can be downloaded at: <https://www.mdpi.com/article/10.3390/inorganics11100387/s1>. Figure S1: ^1H NMR spectrum of **1b** in CDCl_3 , Figure S2: ^1H NMR spectrum of **2b** in CDCl_3 , Figure S3: ^1H NMR spectrum of **3b** in CDCl_3 , Figure S4: $^{13}\text{C}\{^1\text{H}\}$ NMR spectrum of **3b** in CDCl_3 , Figure S5: $^{77}\text{Se}\{^1\text{H}\}$ NMR spectrum of **3b** in CDCl_3 , Figure S6: View of the DFT-optimised S_0 structure of **1b** in the gas phase with atom numbering, Table S1: Selected DFT-calculated metrics for the S_0 state of **1b** in the gas phase and CH_2Cl_2 compared with experimental data from single crystal XRD, Figure S7: View of the DFT-optimised S_0 structure of **2b** in the gas phase with atom numbering, Table S2: Selected DFT-calculated metrics for the T_1 state of complexes **1b** and **2b** in the gas phase, Table S3: Selected DFT-calculated metrics for the S_0 state of **2b** in the gas phase and CH_2Cl_2 compared with experimental data from single crystal XRD, Figure S8: View of the DFT-optimised S_0 structure of **3b** in the gas phase with atom numbering, Table S4: Selected DFT-calculated metrics for the S_0 state of **3b** in the gas phase and CH_2Cl_2 , Figure S9: UV-vis absorption spectra of **1b**, **2b**, and **3b** in CH_2Cl_2 at 298 K, Figure S10: UV-vis absorption spectra of complex **3b** in *tris*-HCl buffer at 298 K, Figure S11: Molecular orbital plots for the DFT-optimised S_0 structure of **1b** in CH_2Cl_2 solution, Figure S12: Molecular orbital plots for the DFT-optimised S_0 structure of **2b** in CH_2Cl_2 solution, Figure S13: Molecular orbital plots for the DFT-optimised S_0 structure of **3b** in CH_2Cl_2 solution, Table S5: Composition and energies of selected molecular orbitals of **1b** in CH_2Cl_2 , Table S6: Composition and energies of selected molecular orbitals of **2b** in CH_2Cl_2 , Table S7: Composition and energies of selected molecular orbitals of **3b** in CH_2Cl_2 , Table S8: Wavelengths and the nature of transitions of complex **1b**, Table S9: Wavelengths and the nature of transitions of complex **2b**, Table S10: Wavelengths and the nature of transitions of complex **3b**.

Author Contributions: Conceptualisation, M.D.A.; methodology, M.D.A., S.M.N. and A.K.; software, M.D.A.; validation, M.D.A., R.B.A. and A.K.; formal analysis, M.D.A., R.B.A. and A.K.; investigation, Z.S., M.D.A. and R.B.A.; resources, M.D.A. and S.M.N.; data curation, Z.S., M.D.A. and R.B.A.; writing—original draft preparation, M.D.A. and S.M.N.; writing—review and editing, M.D.A. and A.K.; visualisation, M.D.A. and R.B.A.; supervision, M.D.A.; project administration, M.D.A., S.M.N. and A.K. All authors have read and agreed to the published version of the manuscript.

Funding: M.D.A. gratefully acknowledges financial support from the Tarbiat Modares University and Iran Science Elites Federation (ISEF). A.K. and S.M.N. acknowledge the Deutsche Forschungsgemeinschaft (DFG), grant KL-1194/19-1.

Institutional Review Board Statement: The work and report are in full agreement with the ethical standards of all three universities and the Deutsche Forschungsgemeinschaft (DFG).

Data Availability Statement: Data is available on request.

Acknowledgments: We thank Hamidreza Shahsavari for his helpful comments.

Conflicts of Interest: We hereby declare that there are no conflict of interest and that this work was conducted solely for academic purposes.

References

1. Wei, Y.-C.; Wang, S.F.; Hu, Y.; Liao, L.-S.; Chen, D.-G.; Chang, K.-H.; Wang, C.-W.; Liu, S.-H.; Chan, W.-H.; Liao, J.-L. Overcoming the energy gap law in near-infrared OLEDs by exciton-vibration decoupling. *Nat. Photonics* **2020**, *14*, 570–577. [[CrossRef](#)]
2. Mills, I.N.; Porras, J.A.; Bernhard, S. Judicious design of cationic, cyclometalated Ir(III) complexes for photochemical energy conversion and optoelectronics. *Acc. Chem. Res.* **2018**, *51*, 352–364. [[CrossRef](#)] [[PubMed](#)]
3. Fleetham, T.; Li, G.; Li, J. Phosphorescent Pt(II) and Pd(II) complexes for efficient, high-color-quality, and stable OLEDs. *Adv. Mater.* **2017**, *29*, 1601861. [[CrossRef](#)] [[PubMed](#)]
4. Prokhorov, A.M.; Hofbeck, T.; Czerwieniec, R.; Suleymanova, A.F.; Kozhevnikov, D.N.; Yersin, H. Brightly luminescent Pt(II) pincer complexes with a sterically demanding carboranyl-phenylpyridine ligand: A new material class for diverse optoelectronic applications. *J. Am. Chem. Soc.* **2014**, *136*, 9637–9642. [[CrossRef](#)] [[PubMed](#)]
5. Büyükekşi, S.I.; Şengül, A.; Erdönmez, S.; Altındal, A.; Orman, E.B.; Özkaya, A.R. Spectroscopic, electrochemical and photovoltaic properties of Pt(II) and Pd(II) complexes of a chelating 1,10-phenanthroline appended perylene diimide. *Dalton Trans.* **2018**, *47*, 2549–2560. [[CrossRef](#)]

6. Goswami, S.; Hernandez, J.L.; Gish, M.K.; Wang, J.; Kim, B.; Laudari, A.P.; Guha, S.; Papanikolas, J.M.; Reynolds, J.R.; Schanze, K.S. Cyclometalated platinum-containing diketopyrrolopyrrole complexes and polymers: Photophysics and photovoltaic applications. *Chem. Mater.* **2017**, *29*, 8449–8461. [[CrossRef](#)]
7. Wenger, O. Vapochromism in organometallic and coordination complexes: Chemical sensors for volatile organic compounds. *Chem. Rev.* **2013**, *113*, 3686–3733. [[CrossRef](#)]
8. De los Santos, Z.A.; Wolf, C. Optical Terpene and Terpenoid Sensing: Chiral Recognition, Determination of Enantiomeric Composition and Total Concentration Analysis with Late Transition Metal Complexes. *J. Am. Chem. Soc.* **2020**, *142*, 4121–4125. [[CrossRef](#)]
9. Choi, W.J.; Choi, S.; Ohkubo, K.; Fukuzumi, S.; Cho, E.J.; You, Y. Mechanisms and applications of cyclometalated Pt(II) complexes in photoredox catalytic trifluoromethylation. *Chem. Sci.* **2015**, *6*, 1454–1464. [[CrossRef](#)]
10. Lang, P.; Habermehl, J.; Troyanov, S.I.; Rau, S.; Schwalbe, M. Photocatalytic Generation of Hydrogen Using Dinuclear π -Extended Porphyrin–Platinum Compounds. *Chem.-Eur. J.* **2018**, *24*, 3225–3233. [[CrossRef](#)]
11. Zhong, J.-J.; To, W.-P.; Liu, Y.; Lu, W.; Che, C.-M. Efficient acceptorless photo-dehydrogenation of alcohols and N-heterocycles with binuclear platinum(II) diphosphite complexes. *Chem. Sci.* **2019**, *10*, 4883–4889. [[CrossRef](#)] [[PubMed](#)]
12. Martynova, E.A.; Voloshkin, V.A.; Guillet, S.G.; Bru, F.; Beliš, M.; Van Hecke, K.; Cazin, C.S.; Nolan, S.P. Energy transfer (EnT) photocatalysis enabled by gold-N-heterocyclic carbene (NHC) complexes. *Chem. Sci.* **2022**, *13*, 6852–6857. [[CrossRef](#)] [[PubMed](#)]
13. Ko, C.-N.; Li, G.; Leung, C.-H.; Ma, D.-L. Dual function luminescent transition metal complexes for cancer theranostics: The combination of diagnosis and therapy. *Coord. Chem. Rev.* **2019**, *381*, 79–103. [[CrossRef](#)]
14. Yip, A.M.-H.; Lo, K.K.-W. Luminescent rhenium(I), ruthenium(II), and iridium(III) polypyridine complexes containing a poly(ethylene glycol) pendant or bioorthogonal reaction group as biological probes and photocytotoxic agents. *Coord. Chem. Rev.* **2018**, *361*, 138–163. [[CrossRef](#)]
15. Zhang, R.; Yuan, J. Responsive metal complex probes for time-gated luminescence biosensing and imaging. *Acc. Chem. Res.* **2020**, *53*, 1316–1329. [[CrossRef](#)] [[PubMed](#)]
16. Shaikh, S.; Wang, Y.; Ur Rehman, F.; Jiang, H.; Wang, X. Phosphorescent Ir(III) complexes as cellular staining agents for biomedical molecular imaging. *Coord. Chem. Rev.* **2020**, *416*, 213344. [[CrossRef](#)]
17. Fernández-Moreira, V.; Thorp-Greenwood, F.L.; Coogan, M.P. Application of d^6 transition metal complexes in fluorescence cell imaging. *Chem. Commun.* **2010**, *46*, 186–202. [[CrossRef](#)]
18. Zhang, K.Y.; Yu, Q.; Wei, H.; Liu, S.; Zhao, Q.; Huang, W. Long-lived emissive probes for time-resolved photoluminescence bioimaging and biosensing. *Chem. Rev.* **2018**, *118*, 1770–1839. [[CrossRef](#)]
19. Li, K.; Chen, Y.; Wang, J.; Yang, C. Diverse emission properties of transition metal complexes beyond exclusive single phosphorescence and their wide applications. *Coord. Chem. Rev.* **2021**, *433*, 213755. [[CrossRef](#)]
20. Hu, J.; Nikraves, M.; Shahsavari, H.R.; Babadi Aghakhanpour, R.; Rheingold, A.L.; Alshami, M.; Sakamaki, Y.; Beyzavi, H. A C^N Cycloplatinated(II) Fluoride Complex: Photophysical Studies and Csp³-F Bond Formation. *Inorg. Chem.* **2020**, *59*, 16319–16327. [[CrossRef](#)]
21. Zaroni, K.P.S.; Coppo, R.L.; Amaral, R.C.; Iha, N.Y.M. Ir(III) complexes designed for light-emitting devices: Beyond the luminescence color array. *Dalton Trans.* **2015**, *44*, 14559–14573. [[CrossRef](#)] [[PubMed](#)]
22. Buil, M.L.; Esteruelas, M.A.; López, A.M. Recent Advances in Synthesis of Molecular Heteroleptic Osmium and Iridium Phosphorescent Emitters. *Eur. J. Inorg. Chem.* **2021**, *2021*, 4731–4761. [[CrossRef](#)]
23. Giménez, N.; Lalinde, E.; Lara, R.; Moreno, M.T. Design of luminescent, heteroleptic, cyclometalated Pt^{II} and Pt^{IV} complexes: Photophysics and effects of the cyclometalated ligands. *Chem.-Eur. J.* **2019**, *25*, 5514–5526. [[CrossRef](#)] [[PubMed](#)]
24. Berenguer, J.R.; Lalinde, E.; Moreno, M.T. Luminescent cyclometalated-pentafluorophenyl Pt^{II}, Pt^{IV} and heteropolynuclear complexes. *Coord. Chem. Rev.* **2018**, *366*, 69–90. [[CrossRef](#)]
25. Kunkely, H.; Vogler, A. Electronic spectra and photochemistry of methyl platinum(IV) complexes. *Coord. Chem. Rev.* **1991**, *111*, 15–25. [[CrossRef](#)]
26. Chassot, L.; Von Zelewsky, A.; Sandrini, D.; Maestri, M.; Balzani, V. Photochemical preparation of luminescent platinum(IV) complexes via oxidative addition on luminescent platinum(II) complexes. *J. Am. Chem. Soc.* **1986**, *108*, 6084–6085. [[CrossRef](#)]
27. Jenkins, D.M.; Bernhard, S. Synthesis and Characterization of Luminescent Bis-Cyclometalated Platinum^{IV} Complexes. *Inorg. Chem.* **2010**, *49*, 11297–11308. [[CrossRef](#)]
28. Katlenok, E.A.; Balashev, K.P. Complexes of Rh(III), Ir(III), and Pt(IV) with Metallated 2-(n-Tolyl)pyridine, Ethylenediamine, Acetate, and Diethyldithiocarbamate Ligands. *Russ. J. Gen. Chem.* **2014**, *84*, 927–933. [[CrossRef](#)]
29. Juliá, F.; Bautista, D.; González-Herrero, P. Developing strongly luminescent platinum(IV) complexes: Facile synthesis of bis-cyclometalated neutral emitters. *Chem. Commun.* **2016**, *52*, 1657–1660. [[CrossRef](#)]
30. Juliá, F.; García-Legaz, M.-D.; Bautista, D.; González-Herrero, P. Influence of Ancillary Ligands and Isomerism on the Luminescence of Bis-cyclometalated Platinum(IV) Complexes. *Inorg. Chem.* **2016**, *55*, 7647–7660. [[CrossRef](#)]
31. Giménez, N.; Lara, R.; Moreno, M.T.; Lalinde, E. Facile Approaches to Phosphorescent Bis(cyclometalated) Pentafluorophenyl Pt^{IV} Complexes: Photophysics and Computational Studies. *Chem.-Eur. J.* **2017**, *23*, 5758–5771. [[CrossRef](#)]
32. Vivancos, Á.; Poveda, D.; Muñoz, A.; Moreno, J.; Bautista, D.; González-Herrero, P. Selective synthesis, reactivity and luminescence of unsymmetrical bis-cyclometalated Pt(IV) complexes. *Dalton Trans.* **2019**, *48*, 14367–14382. [[CrossRef](#)] [[PubMed](#)]

33. Juliá, F.; Bautista, D.; Fernández-Hernández, J.M.; González-Herrero, P. Homoleptic tris-cyclometalated platinum(IV) complexes: A new class of long-lived, highly efficient ^3LC emitters. *Chem. Sci.* **2014**, *5*, 1875–1880. [CrossRef]
34. Juliá, F.; Aullón, G.; Bautista, D.; González-Herrero, P. Exploring Excited-State Tunability in Luminescent Tris-cyclometalated Platinum(IV) Complexes: Synthesis of Heteroleptic Derivatives and Computational Calculations. *Chem.-Eur. J.* **2014**, *20*, 17346–17359. [CrossRef] [PubMed]
35. Juliá, F.; González-Herrero, P. Spotlight on the ligand: Luminescent cyclometalated Pt(IV) complexes containing a fluorenyl moiety. *Dalton Trans.* **2016**, *45*, 10599–10608. [CrossRef] [PubMed]
36. López-López, J.C.; Bautista, D.; González-Herrero, P. Stereoselective Formation of Facial Tris-Cyclometalated Pt^{IV} Complexes: Dual Phosphorescence from Heteroleptic Derivatives. *Chem.-Eur. J.* **2020**, *26*, 11307–11315. [CrossRef]
37. Juliá, F.; González-Herrero, P. Aromatic C–H activation in the triplet excited state of cyclometalated platinum(II) complexes using visible light. *J. Am. Chem. Soc.* **2016**, *138*, 5276–5282. [CrossRef]
38. Poveda, D.; Vivancos, A.; Bautista, D.; Gonzalez-Herrero, P. Visible light driven generation and alkyne insertion reactions of stable bis-cyclometalated Pt(IV) hydrides. *Chem. Sci.* **2020**, *11*, 12095–12102. [CrossRef]
39. Vivancos, A.; Jiménez-García, A.; Bautista, D.; González-Herrero, P. Strongly Luminescent Pt(IV) Complexes with a Mesoionic N-Heterocyclic Carbene Ligand: Tuning Their Photophysical Properties. *Inorg. Chem.* **2021**, *60*, 7900–7913. [CrossRef]
40. López-López, J.-C.; Bautista, D.; González-Herrero, P. Phosphorescent biaryl platinum(IV) complexes obtained through double metalation of dibenzoidolium ions. *Chem. Commun.* **2022**, *58*, 4532–4535. [CrossRef]
41. Zhang, Y.; Meng, F.; You, C.; Yang, S.; Xiong, L.; Xiong, W.; Zhu, W.; Wang, Y.; Pei, Y.; Su, S. Efficient near-infrared emitting tetradentate bis-cyclometalated platinum(IV) complexes for solution-processed polymer light emitting diodes. *Dyes Pigment.* **2017**, *142*, 457–464. [CrossRef]
42. Ionescu, A.; Godbert, N.; Aiello, I.; Ricciardi, L.; La Deda, M.; Crispini, A.; Sicilia, E.; Ghedini, M. Anionic cyclometalated Pt(II) and Pt(IV) complexes respectively bearing one or two 1,2-benzenedithiolate ligands. *Dalton Trans.* **2018**, *47*, 11645–11657. [CrossRef]
43. Lalinde, E.; Lara, R.; López, I.P.; Moreno, M.T.; Alfaro-Arnedo, E.; Pichel, J.G.; Piñeiro-Hermida, S. Benzothiazole-Based Cycloplatinated Chromophores: Synthetic, Optical, and Biological Studies. *Chem.-Eur. J.* **2018**, *24*, 2440–2456. [CrossRef]
44. Monsour, C.G.; Decosto, C.M.; Tafolla-Aguirre, B.J.; Morales, L.A.; Selke, M. Singlet Oxygen Generation, Quenching and Reactivity with Metal Thiolates. *Photochem. Photobiol.* **2021**, *97*, 1219–1240. [CrossRef] [PubMed]
45. Mackay, F.S.; Farrer, N.J.; Salassa, L.; Tai, H.-C.; Deeth, R.J.; Moggach, S.A.; Wood, P.A.; Parsons, S.; Sadler, P.J. Synthesis, characterisation and photochemistry of Pt^{IV} pyridyl azido acetato complexes. *Dalton Trans.* **2009**, 2315–2325. [CrossRef] [PubMed]
46. Harkins, S.B.; Peters, J.C. Unexpected Photoisomerization of a Pincer-type Amido Ligand Leads to Facial Coordination at Pt(IV). *Inorg. Chem.* **2006**, *45*, 4316–4318. [CrossRef] [PubMed]
47. Van Slageren, J.; Klein, A.; Zalis, S. Ligand-to-ligand charge transfer states and photochemical bond homolysis in metal-carbon bonded platinum complexes. *Coord. Chem. Rev.* **2002**, *230*, 193–211. [CrossRef]
48. Kaim, W.; Klein, A.; Hasenzahl, S.; Stoll, H.; Zalis, S.; Fiedler, J. Reactions of New Organoplatinum(II) and -(IV) Complexes of 1,4-Diaza-1,3-butadienes with Light and Electrons. Emission vs Photochemistry and the Electronic Structures of Ground, Reduced, Oxidized, and Low-Lying Charge-Transfer Excited States. *Organometallics* **1998**, *17*, 237–247. [CrossRef]
49. Hux, J.E.; Puddephatt, R.J. Photochemistry of mononuclear and binuclear tetramethylplatinum(IV) complexes: Reactivity of an organometallic free radical. *J. Organomet. Chem.* **1992**, *437*, 251–263. [CrossRef]
50. Hux, J.E.; Puddephatt, R.J. Photochemistry of tetramethyl(2,2'-bipyridine)platinum(IV). *J. Organomet. Chem.* **1988**, *346*, C31–C34. [CrossRef]
51. Steel, H.L.; Allinson, S.L.; Andre, J.; Coogan, M.P.; Platts, J.A. Platinum trimethyl bipyridyl thiolates—New, tunable, red-to near IR emitting luminophores for bioimaging applications. *Chem. Commun.* **2015**, *51*, 11441–11444. [CrossRef]
52. Mala, B.; Murtagh, L.E.; Farrow, C.M.A.; Akien, G.R.; Halcovich, N.R.; Allinson, S.L.; Platts, J.A.; Coogan, M.P. Photochemical Oxidation of Pt(IV)Me₃(1,2-diimine) Thiolates to Luminescent Pt(IV) Sulfates. *Inorg. Chem.* **2021**, *60*, 7031–7043. [CrossRef]
53. Taylor, S.D.; Shingade, V.M.; Muvirimi, R.; Hicks, S.D.; Krause, J.A.; Connick, W.B. Spectroscopic Characterization of Platinum(IV) Terpyridyl Complexes. *Inorg. Chem.* **2019**, *58*, 16364–16371. [CrossRef]
54. Dogan, A.; Kavakli, C.; Sieger, M.; Niemeyer, M.; Sarkar, B.; Kaim, W. Structural and spectroscopic evidence for marginal metal-to-ligand charge transfer in complexes Pt(abpy)Me₃X, abpy = 2,2'-azobispyridine, X = Cl, Br, I.Z. *Anorg. Allgem. Chem.* **2008**, *634*, 2527–2531. [CrossRef]
55. Van Slageren, J.; Stufkens, D.J.; Zális, S.; Klein, A. Influence of the variation of the co-ligands on the electronic transitions and emission properties of [Pt(I)(CH₃)₃(iPr-DAB)], [Pt(CH₃)₄(α -diimine)] and [Pt(SnPh₃)₂(CH₃)₂(iPr-DAB)]: An experimental and theoretical study. *J. Chem. Soc. Dalton Trans.* **2002**, 218–225. [CrossRef]
56. Bonnington, K.J.; Jennings, M.C.; Puddephatt, R.J. Oxidative Addition of S–S Bonds to Dimethylplatinum(II) Complexes: Evidence for a Binuclear Mechanism. *Organometallics* **2008**, *27*, 6521–6530. [CrossRef]
57. Panunzi, A.; Roviello, G.; Ruffo, F. Fine-Tuning the Basicity of Metal Complexes: Reversible Oxidative Addition of Se–Se Bonds to Platinum(II) Precursors. *Organometallics* **2002**, *21*, 3503–3505. [CrossRef]
58. Cauty, A.J.; Jin, H.; Skelton, B.W.; White, A.H. Oxidation of Complexes by (O₂CPh)₂ and (ER)₂ (E = S, Se), Including Structures of Pd(CH₂CH₂CH₂CH₂)(SePh)₂(bpy) (bpy = 2,2'-Bipyridine) and MMe₂(SePh)₂(L₂) (M = Pd, Pt; L₂ = bpy, 1,10-Phenanthroline) and C \cdots O and C \cdots E Bond Formation at Palladium(IV). *Inorg. Chem.* **1998**, *37*, 3975–3981. [CrossRef]

59. Aye, K.-T.; Vittal, J.J.; Puddephatt, R.J. Oxidative addition of E–E bonds (E = Group 16 element) to platinum(II): A route to platinum(IV) thiolate and selenolate complexes. *J. Chem. Soc. Dalton Trans.* **1993**, 1835–1839. [[CrossRef](#)]
60. Osakada, K. Chemistry of Transition Metal Complexes with Group 16 Elements: Transition Metal Complexes with Two Lone Pairs of Electrons on the Coordinating Atom. In *Organometallic Chemistry*; Nakazawa, H., Koe, J., Eds.; Royal Society of Chemistry: London, UK, 2021; Volume 11, pp. 203–227.
61. He, M.; Ching, H.Y.V.; Policar, C.; Bertrand, H.C. Rhenium tricarbonyl complexes with arenethiolate axial ligands. *New J. Chem.* **2018**, *42*, 11312–11323. [[CrossRef](#)]
62. Klein, A.; Van Slageren, J.; Zalis, S. Co-Ligand Involvement in Ground and Excited States of Electron-Rich (Polypyridyl)Pt^{II} Complexes. *Eur. J. Inorg. Chem.* **2003**, *2003*, 1927–1938. [[CrossRef](#)]
63. Ishida, H.; Tobita, S.; Hasegawa, Y.; Katoh, R.; Nozaki, K. Recent advances in instrumentation for absolute emission quantum yield measurements. *Coord. Chem. Rev.* **2010**, *254*, 2449–2458. [[CrossRef](#)]
64. Armarego, W.L. *Purification of Laboratory Chemicals*, 8th ed.; Elsevier: Amsterdam, The Netherlands, 2017.
65. Becke, A. Density-functional thermochemistry. III The role of exact exchange. *J. Chem. Phys.* **1993**, *98*, 5648–5652. [[CrossRef](#)]
66. Miehlich, B.; Savin, A.; Stoll, H.; Preuss, H. Results obtained with the correlation energy density functionals of Becke and Lee, Yang and Parr. *Chem. Phys. Lett.* **1989**, *157*, 200–206. [[CrossRef](#)]
67. Lee, C.; Yang, W.; Parr, R.G. Development of the Colle-Salvetti correlation-energy formula into a functional of the electron density. *Phys. Rev. B* **1988**, *37*, 785–789. [[CrossRef](#)]
68. Frisch, M.; Trucks, G.; Schlegel, H.; Scuseria, G.; Robb, M.; Cheeseman, J.; Scalmani, G.; Barone, V.; Mennucci, B.; Petersson, G.; et al. *Gaussian 09, Revision D. 01*; Gaussian, Inc.: Wallingford, CT, USA, 2009.
69. Wadt, W.R.; Hay, P.J. Ab initio effective core potentials for molecular calculations. Potentials for main group elements Na to Bi. *Chem. Phys.* **1985**, *82*, 284–298. [[CrossRef](#)]
70. Roy, L.E.; Hay, P.J.; Martin, R.L. Revised basis sets for the LANL effective core potentials. *J. Chem. Theory Comput.* **2008**, *4*, 1029–1031. [[CrossRef](#)]
71. Cossi, M.; Scalmani, G.; Rega, N.; Barone, V. New developments in the polarizable continuum model for quantum mechanical and classical calculations on molecules in solution. *Chem. Phys.* **2002**, *117*, 43–54. [[CrossRef](#)]
72. Barone, V.; Cossi, M.; Tomasi, J. A new definition of cavities for the computation of solvation free energies by the polarizable continuum model. *Chem. Phys.* **1997**, *107*, 3210–3221. [[CrossRef](#)]
73. Zhurko, G.; Zhurko, D. *Chemcraft, Version 1.7*; Informer Technologies, Inc.: Redwood City, CA, USA, 2013.
74. O’Boyle, N.M.; Tenderholt, A.L.; Langner, K.M. cclib: A library for package-independent computational chemistry algorithms. *J. Comput. Chem.* **2008**, *29*, 839–845. [[CrossRef](#)]

Disclaimer/Publisher’s Note: The statements, opinions and data contained in all publications are solely those of the individual author(s) and contributor(s) and not of MDPI and/or the editor(s). MDPI and/or the editor(s) disclaim responsibility for any injury to people or property resulting from any ideas, methods, instructions or products referred to in the content.